

NEUROSYSTEMS

Consistent sequential activity across diverse forms of UP states under ketamine anesthesia

Artur Luczak^{1,2} and Peter Barthó^{2,3}¹Canadian Centre for Behavioural Neuroscience, University of Lethbridge, 4401 University Drive, Lethbridge, AB, Canada, T1K 3M4²Center for Molecular and Behavioral Neuroscience, Rutgers University, Newark, NJ, USA³Institute of Experimental Medicine, Hungarian Academy of Sciences, Budapest, Hungary**Keywords:** rat, sequences of activity, somatosensory cortex

Abstract

During slow-wave sleep, the neocortex shows complex, self-organized spontaneous activity. Similar slow-wave oscillations are present under anesthesia where massive, persistent network activity (UP states) alternates with periods of generalized neural silence (DOWN states). To investigate the neuronal activity patterns occurring during UP states, we recorded simultaneously from populations of cells in neocortical layer V of ketamine/xylazine-anesthetized rats. UP states formed a diverse class. In particular, simultaneous-onset UP states were typically accompanied by sharp field potentials and 10–14 Hz modulation, and were often grouped in a 3 Hz ('delta') pattern. Longer, slow-onset UP states did not exhibit 10–14 Hz modulation, and showed a slow propagation across recording electrodes ('traveling waves'). Despite this diversity, the temporal patterns of spiking activity were similar across different UP state types. Analysis of cross-correlograms revealed conserved temporal relationships among neurons, with each neuron having specific timing during UP states. As a group, putative interneurons were most active at the beginning of UP states and putative pyramidal cells were active uniformly throughout the duration of UP states. These results show that UP states under ketamine anesthesia have a stable, fine-structured firing pattern despite a large variability in global structure.

Introduction

The activity of the cortex, even in primary sensory areas, is not simply a reflection of sensory input (Harris, 2005). Indeed, even when sensory input is absent, such as during sleep, the cortex exhibits complex self-generated and often rhythmic activity (Buzsáki & Draguhn, 2004). Its complex nature and general similarity with activity evoked by sensory input (Tsodyks *et al.*, 1999; Kenet *et al.*, 2003; MacLean *et al.*, 2005; Luczak *et al.*, 2009), suggest that spontaneous activity may play an important role in information processing (Buzsáki, 1989; Destexhe & Sejnowski, 2001; Steriade & Timofeev, 2003). During slow-wave sleep, spontaneous cortical activity is dominated by low-frequency oscillatory patterns, including sleep spindles (transient 7–15 Hz oscillations), K-complexes (sharp potentials often followed by spindle-like oscillation), delta oscillations (1–4 Hz) and slow oscillations (< 1 Hz) consisting of an alternation between UP states, interspersed with DOWN states of generalized silence. Although the function of these low-frequency oscillatory patterns is not yet fully clear (Vertes, 2004), they have been hypothesized to underlie information transfer between cortical networks required for the consolidation of learning (Sirota *et al.*, 2003).

Under anesthesia, the brain exhibits low-frequency patterns homologous to those seen in sleep (Steriade, 2001). *In vivo* studies with anesthetized animals have indicated that slow oscillation arises from recurrent excitation in neocortical circuits (Steriade *et al.*, 1993a). During the UP state, cortical neurons receive a barrage of excitatory and inhibitory input, leading to sustained firing. However, as the UP state progresses, processes such as synaptic depression and buildup of outward currents lower the excitability of the network to the point where activity can no longer be self-sustained, at which point the DOWN state begins. Scalp electroencephalography recordings have shown that, during natural sleep, the UP state propagates across the cortical surface (Massimini *et al.*, 2004). Spindle and delta oscillations, by contrast, are more globally coordinated, and appear to arise from the cooperative action of thalamocortical networks (Steriade *et al.*, 1993b). K-complexes and associated spindles (Amzica & Steriade, 1998) may be triggered by sensory inputs (Ujjaszsi & Halasz, 1986) or a sudden transition to the UP state. Slice models have proved useful in determining the cellular mechanisms of these oscillations. In cortical slice preparations, UP states have been observed to propagate as traveling waves at speeds of ~10 mm/s, spread through lateral cortico-cortical connections (Sanchez-Vives & McCormick, 2000). Other investigators, using a different artificial cerebrospinal fluid solution, have observed briefer, non-traveling UP states involving smaller numbers of neurons (Mao *et al.*, 2001; Cossart *et al.*, 2003). Large-scale optical recordings have revealed that the subsets of neurons involved in these UP states are highly

Correspondence: A. Luczak, ¹Canadian Centre for Behavioural Neuroscience, as above. E-mail: luczak@uleth.ca

Received 18 January 2010, revised 24 May 2012, accepted 28 May 2012

non-random, are predominantly layer V pyramidal neurons, and exhibit intricate but repeatable sequences of activation at UP state onset (Mao *et al.*, 2001; Cossart *et al.*, 2003).

In this study we investigated the network-level structure of spontaneous neocortical activity *in vivo*. We recorded large populations of neurons, together with field potentials, in layer V of the somatosensory cortex in ketamine/xylazine-anesthetized rats using multi-site silicon microelectrodes. We found that spontaneous activity periods form a diverse class, ranging from long-duration UP states spreading mainly as traveling waves, to shorter UP states accompanied by sharp field potentials and spindle-frequency oscillation, which occurred rhythmically at delta frequency. During the DOWN–UP state transition, amongst pyramidal cells, a diversity of temporal relationships to activity onset was seen, revealing complex sequences of activity at the onset of active periods. Although the relative involvement of putative pyramidal cells and interneurons differed with the UP state types, the sequence of cell activation was similar, suggesting that, although the mechanisms of spread of activity in the cortex may vary, its local spatiotemporal structure is highly stereotyped.

Materials and methods

Surgery and recording

A detailed description of the surgery and recording procedures have been published previously (Bartho *et al.*, 2004; Luczak *et al.*, 2007; Gomez Palacio Schjetnan & Luczak, 2011). In summary, three rats of the Sprague-Dawley strain (400–900 g) were anesthetized with a mixture (2 mL/kg) of ketamine (50 mg/mL) and xylazine (2.5 mg/mL) injected intraperitoneally. Rats were placed in a stereotaxic frame, and using stereotaxic coordinates a window in the scalp was prepared over the somatosensory cortex.

In two experiments, we used a silicon probe consisting of eight shanks (200 μm shank separation); each shank had eight recording sites (160 μm^2 site area; 1–3 M Ω impedance) with the recording sites staggered to provide a two-dimensional arrangement (20 μm vertical separation; Fig. S1A). In the third experiment, we used a four-shank silicon probe (200 μm shank separation) with four recording sites at each shank. The silicon probes were manufactured by NeuroNexus Technologies (Ann Arbor, MI, USA, <http://www.neuronexustech.com>). Extracellular signals were high-pass filtered (1 Hz) and amplified (1000 times) using a 64-channel amplifier (Sensorium, Charlotte, VT, USA). Data were digitized at 25 kHz (DataMax System, RC Electronics, Santa Barbara, CA, USA) and 20 kHz (United Electronic Industries, Inc., Canton, MA, USA) in the third experiment. The location of the recording sites was determined to be layer V, based on histological reconstruction of the electrode tracks (Bartho *et al.*, 2004), electrode depth, and firing patterns. Units were identified and isolated by a semiautomatic ‘cluster cutting’ algorithm (Harris *et al.*, 2000) (available at: <http://www.klustakwik.sourceforge.net>), followed by manual clustering (<http://www.klusters.sourceforge.net>). Multi-unit activity, clusters with low separation quality (isolation distance < 20) (Harris *et al.*, 2000; Schmitzer-Torbert *et al.*, 2005) or firing rates lower than 0.3 Hz were excluded from analysis. From over 400 recorded cells, 241 well-isolated neurons passed the criteria for further analyses. Examples of average spike waveforms of identified neurons on a single recording shank are shown in Fig. S1B.

After the experiment, the rats were injected with sodium pentobarbital (0.5 ml i.p. of 320 mg/ml). Once non-responsive, the animals were perfused transcardially with physiological saline and 10% formalin. All experiments were carried out in accordance with

protocols approved by the Rutgers University Animal Care and Use Committee and conformed to NIH Guidelines on the Care and Use of Laboratory Animals.

Discrimination of putative interneurons and putative pyramidal cells

Narrow-spike cells (putative interneurons) and wide-spike cells (putative pyramidal cells) in the neocortex can be characterized by distinct extracellular spike waveform features. Although spike width cannot always unequivocally discriminate between interneurons and pyramidal cells, it is generally accepted that, for the vast majority of neurons, it is a valid and useful indicator of cell type (Constantinidis & Goldman-Rakic, 2002; Viskontas *et al.*, 2007; Yokota *et al.*, 2010). We used spike duration (measured as trough to peak time in the spike waveform) and half-amplitude duration to determine the type of neuron (Fig. S1C, top inset). The distribution of spike widths was bimodal (Fig. S1C). Based on the examination of this distribution and previously published results (Bartho *et al.*, 2004), neurons with a spike duration shorter than 0.55 ms in unfiltered traces were classified as putative fast-spiking interneurons. From three experiments, we had a total of 215 well-isolated wide-spike cells and 26 narrow-spike cells.

For verification of this classification procedure, we computed cross-correlograms (1 ms bin width) between all pairs of recorded neurons to identify inhibitory and excitatory connections. Significant peaks within 3 ms of the center bin were considered as putative monosynaptic connections. A peak in the cross-correlogram was defined as significant when at least one of the bins exceeded 99.9% (mean + 3 SD) of the bin values in the control period calculated between –30 and –10 ms and between +10 and +30 ms (Fig. S1C, bottom inset). Similarly, short-latency troughs were considered to be due to inhibition when at least two neighboring 1 ms bins were < 0.1% of values in the control period (Fig. S1C, middle inset). For cell pairs recorded from the same electrode, the 0 and 1 ms bins were not considered, due to the possibility of overlapping spikes (Bartho *et al.*, 2004; Luczak *et al.*, 2007). In our dataset, in cross-correlograms showing monosynaptic inhibition, triggering neurons always had narrow spikes, whereas in cross-correlograms showing monosynaptic excitation, triggering neurons always had wide spikes (Fig. S1C, filled circles). These findings provide strong evidence for the validity of classification based on spike width in this dataset.

To further examine spike width-based classification, we also investigated the firing patterns of putative interneurons and putative pyramidal cells (Fig. S2). Consistently with previous findings, most neurons identified as putative interneurons had higher firing rates and shorter interspike intervals, characteristic of GABAergic fast-spiking cells (Kawaguchi & Kubota, 1997).

Detection of UP states

The UP states were identified from the spiking activity of all recorded cells. We defined the beginning of an UP state as the time of the first spike marking a transition from a period of global silence (30 ms with at most one spike of any cell) to a period of activity (60 ms with at least 15 spikes from all cells). The end of the UP state was defined as the time of the last spike marking a transition to at least 30 ms of silence. UP states shorter than 60 ms, or containing fewer than 50 spikes from all neurons, were excluded from further analysis. To ensure that our results were not due to these particular criteria, we repeated the analysis using different parameter values (the required

number of spikes in the pre-UP state time window was varied between 0 and 2, and the number of spikes in the following window was varied from 5 to 25). These changes resulted in a different number of detected UP states (change within $\pm 10\%$) but did not affect our findings in essence.

The first peak and second peak amplitude

To characterize the local field potential (LFP) pattern accompanying UP state onsets, we calculated two quantities – the ‘first peak amplitude’ measuring the size of the initial transient, and the ‘second peak amplitude’ characterizing subsequent ~ 12 Hz oscillation from LFPs averaged across all electrodes. For each UP state, the first peak amplitude was defined as the difference between the amplitude of the LFP at the beginning of the UP state and the minimum LFP amplitude within 100 ms after the UP state began (see Fig. 1C). The ‘second peak amplitude’ was defined as the size of the second oscillation cycle, measured by the maximum peak-to-trough amplitude in a range of 20–150 ms after the initial LFP minimum (see Fig. 1C).

To verify that our results were not specific to these particular definitions, we repeated the analysis using two other definitions of the first peak amplitude. First, because averaging across electrodes may alter the results when peak times differ between sites, we calculated the peak amplitude as described above for every electrode separately, and took the maximum value. Second, we calculated the first peak amplitude as the minimum LFP amplitude within 100 ms after the beginning of the UP state relative to baseline. This definition is less dependent on finding the precise time that the UP state began. Neither redefinition affected our results.

To quantify the modulation of spiking activity by the spindle-frequency oscillation for each neuron, we calculated the ‘second peak modulation’. This measure was defined as the ratio of the mean firing rate during the trough between the two LFP peaks (70–85 ms after UP state onset) to the mean firing rate during the second peak (95–120 ms after UP state onset).

Propagation slope

To determine the speed of propagation of UP state onset across recording shanks, we calculated for each shank the median time of the first five spikes of any cell after the UP state began, and fitted a least squares line to these times as a function of shank location. The values of the slope were consistent if the number of spikes used to compute the median onset time was varied from 3 to 10.

Latency

To quantify the temporal relationship between a neuron and the population activity during different types of UP states, we assessed the asymmetry of the spike-triggered multi-unit activity using a previously described latency measure, defined as the mean spike time of the spike-triggered multi-unit activity within a 100 ms time window. It was equivalent to calculating the center of mass of a cross-correlogram (Luczak *et al.*, 2009). Before calculating the center of mass, cross-correlograms were normalized between 0 and 1 to discard the effect of baseline activity. Analyses were repeated, computing the latency using multi-unit activity taken only from each neuron’s local recording shank. For all datasets, this resulted in changes in latency of $< 5\%$, indicating that consistent timing differences between neurons arise

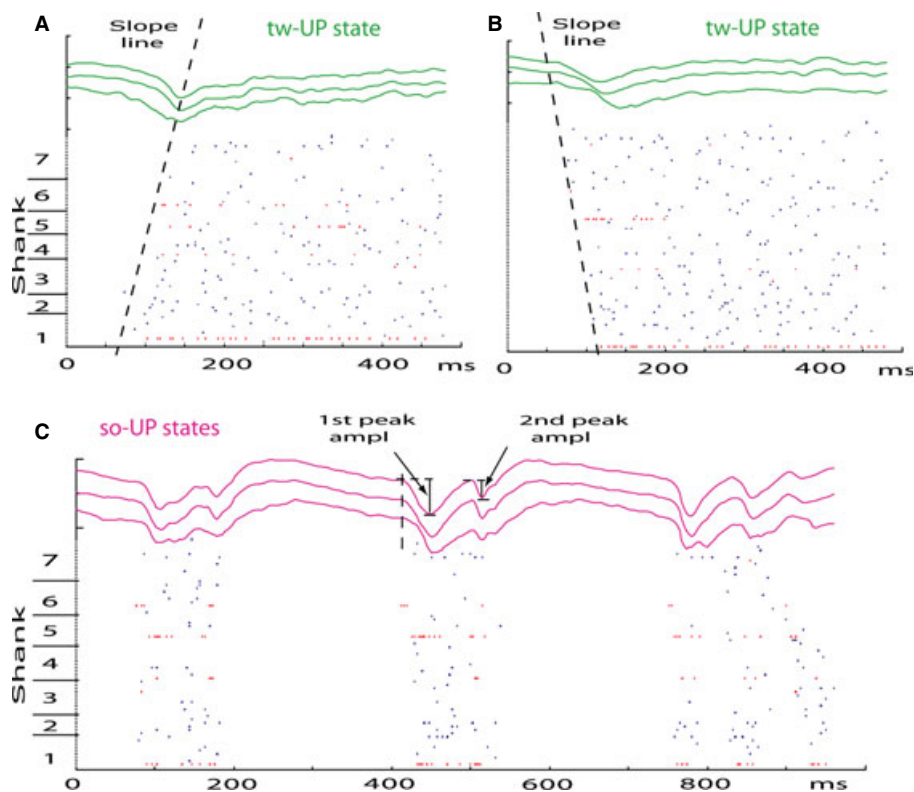


FIG. 1. Raster plots of the beginning of UP states. (A) tw-UP state with neuronal activity spreading from shank 1 to shank 7. Narrow-spike cells are denoted in red, and the dashed line illustrates the slope of activity propagation. On top are LFP traces from shanks 1, 4, and 7. (B) Example of a tw-UP state propagating in the opposite direction. (C) so-UP states.

within the local circuit rather than from the spatial spread of activity across multiple shanks (Luczak *et al.*, 2007).

Results

To study the fine structure of neural coordination during spontaneous activity, we recorded neuronal populations in layer V of the neocortex using multi-site silicon microelectrodes in ketamine/xylazine-anesthetized rats. Visual inspection revealed a striking coordination of activity, with prolonged periods of silence for all recorded neurons alternating with spontaneously active periods (UP states) where spiking was seen at all recording sites (Fig. 1). UP state onset was accompanied by a depth-negative LFP, whereas silent periods were characterized by dome-shaped depth-positive LFP. Closer inspection of UP states revealed a diversity of patterns. Some UP states exhibited a progressive spread of activation across sites (Fig. 1A and B). They tended to be long-lasting, ranging up to a maximum length of 2–3 s. Their onset was marked by a single negative LFP peak, which occurred for each shank at the time of the spiking onset. Other UP states exhibited near-simultaneous onset at all sites. These tended to be shorter in duration (around 200 ms), and were accompanied by larger LFP negativity, frequently modulated at ~ 12 Hz (Fig. 1C). We term these two types of patterns ‘traveling-wave’ UP (tw-UP) states, and ‘simultaneous-onset’ UP (so-UP) states, respectively (see next section for exact definition).

We quantified these trends using several parameters, such as the amplitude of the initial negative LFP deflection, the amplitude of the second deflection occurring at 20–150 ms after the first peak (indicating the power of spindle oscillation, or the lack of it), and the speed of spatial propagation of UP states between recording sites (see Materials and methods for details and Fig. 1A and B for illustration). UP states formed a continuum between short, near-simultaneous-onset events accompanied by modulation at spindle frequency, and longer-lasting events that spread more slowly across the recorded area, and were accompanied by smaller monophasic onset potentials (Fig. 2A–C).

To analyze in more detail the similarities and differences between the two extremes of this continuum of UP state type, we divided the UP states into subgroups with the first peak amplitudes > 2.5 mV (so-UP states) and smaller than 1.5 mV (tw-UP states). Figure 2D illustrates representative examples of LFPs from a single shank for periods classified as tw-UP states and so-UP states (denoted by green and pink colors, respectively). To verify that this UP state classification based on the first peak amplitude was also relevant for spiking activity, we calculated the average autocorrelogram from all cells separately for so-UP states and tw-UP states (Fig. 2E) (detailed analysis of spiking activity is presented in the following sections). Consistently with LFP analyses, neurons during so-UP states had strong second peaks in the autocorrelogram, which were absent for tw-UP states. Timing of this second peak in the autocorrelogram was around spindle frequency (80–90 ms), similar to the time between the first and second peak in so-UP states (Fig. 2F).

The presence of propagating waves during tw-UP states was verified statistically by recomputing the propagation slope after shuffling the shank order. The distributions of absolute values of the slope for shuffled and non-shuffled shank orders were significantly different ($P < 0.01$; Kolmogorov–Smirnov test; Fig. 2G). The activity could propagate in either direction across recording shanks, and showed little directional preference. The signed mean direction of UP state propagation was < 1.4 ms/shank (shank refers to 200 μm , a distance between two consecutive shanks), compared with the overall

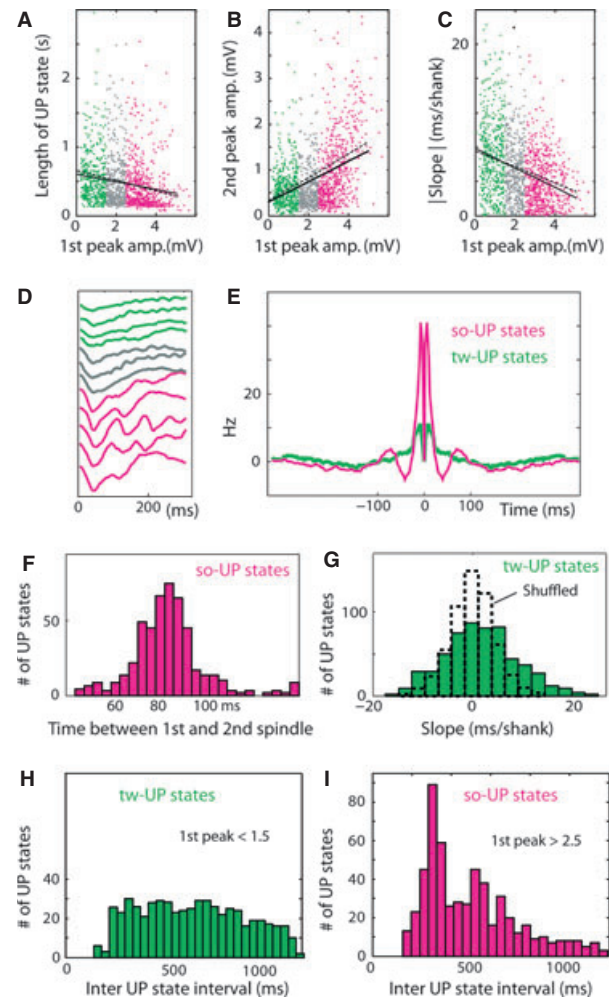


FIG. 2. Characterizing so-UP states and tw-UP states. (A) First peak amplitude of LFP vs. length of UP state. The regression line shows negative correlation between the first peak amplitude and length of UP state ($R = -0.33$, $P < 0.0001$). Here and henceforth, pink and green colors will denote so-UP states (first peak amplitude > 2.5 mV) and tw-UP states (first peak amplitude smaller than 1.5 mV), respectively. (B) UP states with a large first peak amplitude tend to also have a larger second LFP peak characteristic of spindle-frequency modulation ($R = 0.39$, $P < 0.0001$). (C) First peak amplitude vs. absolute value of the slope shows that UP states with a smaller first peak amplitude travel more slowly between recording sites ($R = -0.28$, $P < 0.0001$). In A–C, dashed lines show the regression line after recalculating the peak's amplitude from a single shank with the largest deflection ($R_{1\text{st peak} - \text{length}} = -0.34$, $P < 0.0001$; $R_{1\text{st-2nd peak}} = 0.41$, $P < 0.0001$; $R_{1\text{st peak} - \text{slope}} = -0.28$, $P < 0.0001$). (D) Representative examples of UP state-triggered LFPs sorted by first peak amplitude from a single shank. (E) Average autocorrelogram of single unit activity during so-UP states (pink) and tw-UP states (green). For figure clarity, the value of the autocorrelogram at time 0 was set to 0. (F) Histogram of times between the first and second LFP peak for so-UP states. (G) Histogram of slopes for tw-UP states. The dashed line shows the distribution of slopes for shank shuffled data. The slope of 0 ms/shank corresponds to the simultaneous occurrence of UP state at all shanks, and the slope of 20 ms/shank corresponds to a propagation speed of traveling waves of 10 mm/s. Note that only for waves that travel in a direction parallel to the shanks does the estimated slope correspond to the actual speed of wave propagation. (H) Histograms of inter-UP state intervals for tw-UP states and so-UP states in I. Peak in the histogram in I at around 300 ms corresponds to so-UP states recurring at delta frequency.

span of the slope values (-16 to $+23$ ms/shank). The UP states with the largest slopes (most likely to travel in the direction parallel to the recording shanks) reached a maximum absolute delay of about 150 ms

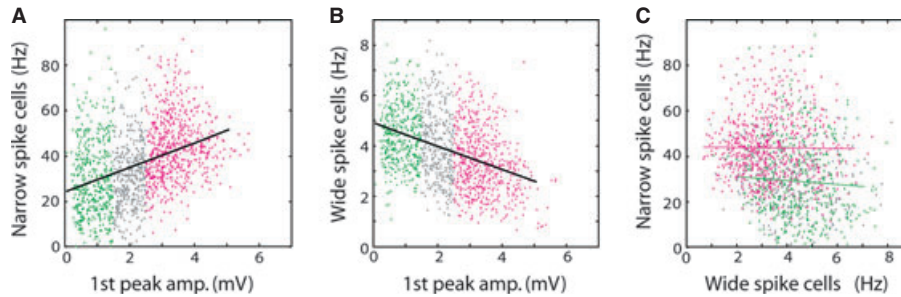


FIG. 3. Mean firing rate of narrow-spike cells (putative interneurons) and wide-spike cells (putative pyramidal cells) during UP states. Every point represents the mean rate averaged over all recorded neurons of the appropriate class, during the first peak period (20–60 ms) of a single UP state. (A) Mean rate of narrow-spike cells is larger for UP states of large first peak amplitude. (B) In contrast, the mean rate of wide-spike cells decreases with the first peak amplitude. (C) Scatter plot of narrow-spike vs. wide-spike rates for all UP states. Across all UP state types, the firing rate of narrow-spike cells is negatively correlated with the firing rate of wide-spike cells; however, within a single UP state type, no correlation is observed.

to span 1.4 mm between the furthest recording shanks. This finding suggests a propagation speed of approximately 10 mm/s. Note that we can estimate the speed of wave propagation most reliably only for waves that travel parallel to the shanks. When recording with eight-site probes, we occasionally observed waves that could be seen only on the few leftmost or rightmost shanks. However, in the majority of cases (~95%) the UP state traveled across all shanks. The tw-UP states occurred at slow frequencies ranging uniformly from below 1 Hz up to 4 Hz (Fig. 2H). In contrast, during so-UP states, we frequently observed a series (ranging from 3 up to 10) of short-lasting (~200 ms) so-UP states, accompanied by large field potential deflection, recurring at ~3 Hz (delta) frequency (Figs 1C and 2I).

To investigate whether the diversity in UP state structure might correlate with differential participation of neuronal classes, we distinguished putative fast-spiking interneurons and putative pyramidal cells on the basis of extracellular spike width, firing patterns and analysis of monosynaptic interactions (Materials and methods) (Bartho *et al.*, 2004). First, the peak amplitude and second peak amplitude were positively correlated with the firing rate of putative interneurons ($R = 0.39$; $P < 0.001$; $n = 1423$ UP states; Fig. 3A), but negatively correlated with the firing rate of putative pyramidal cells ($R = -0.41$; $P < 0.001$; $n = 1423$ UP states; Fig. 3B). When considering all UP states, the mean rate of putative pyramidal cells was negatively correlated with that of putative interneurons (Fig. 3C). Within each UP state group, however, the correlation between the firing rates of narrow-spike and wide-spike cells was not significant ($P > 0.1$; Fig. 3C), suggesting that the negative correlation was due to the differential effect of UP state type.

The temporal structure of activity within the UP state also varied between cell classes. All recorded putative interneurons displayed similar temporal activity profiles. For so-UP states, interneuron firing was strongly modulated at spindle frequency, showing strong peaks of activity for each LFP trough (Fig. 4A and C). For tw-UP states, a temporal profile of interneuron firing consisted of a single, broader peak of lower firing rate and with a similar temporal order of activation as for so-UP states (Fig. 4B and D). Putative pyramidal cells displayed a diversity of temporal profiles even for the same UP state type (examples are given in Fig. 4E–H). Figure 4G represents examples of perievent time histograms (PETHs) calculated for so-UP states from three different pyramidal cells. The two upper cells in Fig. 4G show similar locking to the modulation at spindle frequency as do putative interneurons. By contrast, the bottom cell in Fig. 4G has a peak of activity during the decrease in firing rate of putative interneurons. Principal component analysis of putative pyramidal cell PETHs did not reveal discrete clusters, but rather revealed a

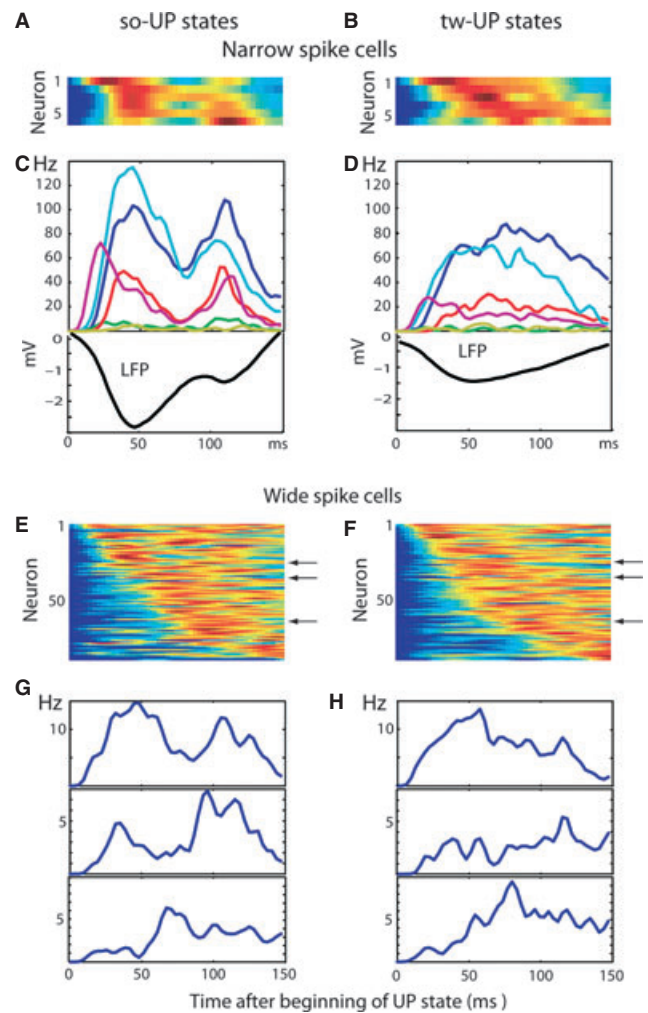


FIG. 4. Average single unit activity during so-UP states (left column) and tw-UP states (right column). (A and B) Average normalized activity of six putative interneurons; each row represents one neuron. Neurons are arranged vertically in the same order in both plots, by increasing latency averaged over all UP states (see Material and methods). (C and D) PETHs of the same neurons (smoothed with a 15 ms Gaussian kernel), with mean LFP shown below. During so-UP states, narrow-spike cells are strongly modulated by the field potential. (E and F) Average normalized activity of putative pyramidal cells sorted by latency averaged over all UP states. Again, neurons are arranged in the same vertical order in both plots. (G and H) Examples of average activity of three wide-spike cells (positions indicated by arrows in E and F). Some wide-spike cells show field-related modulation, but temporal modulation among wide-spike cells is highly variable.

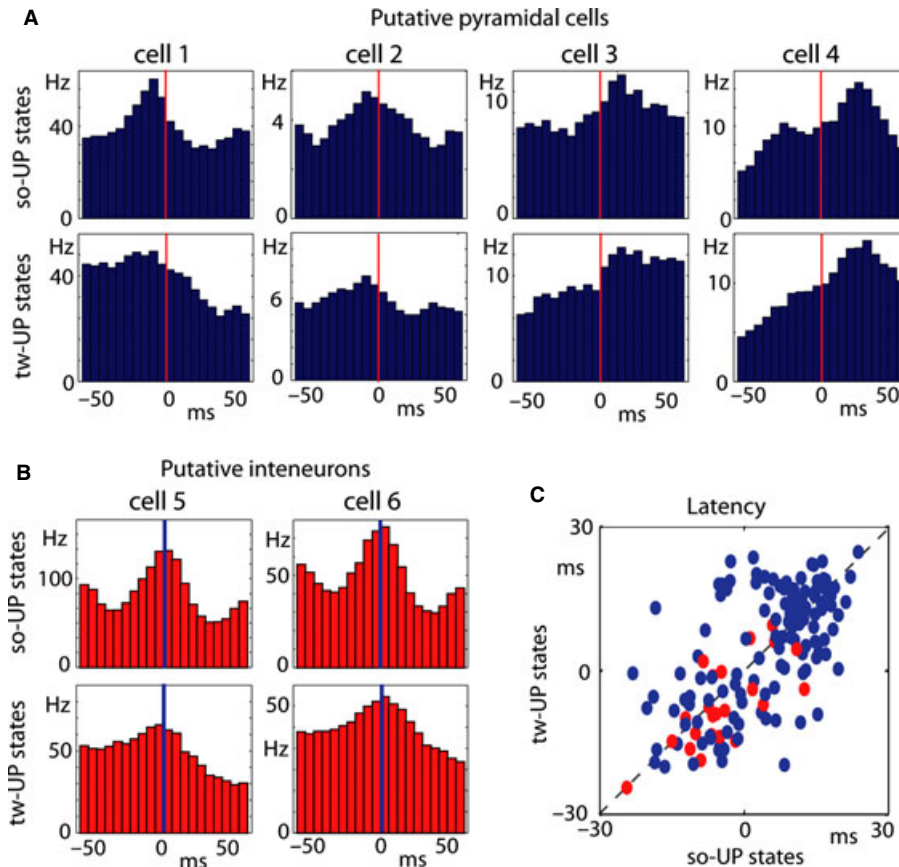


FIG. 5. Neurons have similar cross-correlograms during tw-UP states and so-UP states. (A) Cross-correlogram between a single neuron and multi-unit activity (see Materials and methods) during the first 150 ms of UP states for putative pyramidal cells (activity of the analyzed cell is triggered at multi-unit activity spikes). Note that each cell has a different timing relation to multi-unit activity but that the timing relation is similar for so-UP states and tw-UP states. (B) The same analysis for putative interneurons. As compared with putative pyramidal cells, putative interneurons show a less diverse timing in relation to multi-unit activity. (C) Comparison of latencies calculated for so-UP states and tw-UP states (latency is defined as the center of mass of the cross-correlogram; see Materials and methods). Red and blue dots denote putative interneurons and putative pyramidal cells, respectively. Distribution of points along the identity line (dashed line) shows that, regardless of the UP state type, neurons have a consistent temporal relation to population activity.

continuum of PETH shapes (not shown). Interestingly, the PETH shapes of putative pyramidal neurons for the two UP state types were related (Fig. 4E and F).

To examine in more detail the temporal relationship between the activity of neurons during different types of UP states, for each neuron we calculated its cross-correlogram with the summed activity of all other neurons (Fig. 5A and B). Consistent with the findings illustrated in Fig. 4A,B,E, and F, the activity profiles of the neurons were similar for tw-UP states and so-UP states, with putative pyramidal cells showing a much wider diversity of temporal patterns than putative interneurons (Fig. 5A and B). To quantify this, we summarized each neuron's cross-correlograms by a single parameter called latency (the center of mass of a cross-correlogram; see Materials and methods). We found that neurons had consistent latency across UP state types (Fig. 5C; $R = 0.59$, $P < 0.01$). However, this latency was not correlated with the vertical position of the neuron, as estimated by the location of the recording site with the largest extracellular amplitude ($P = 0.54$), or with the mean firing rate ($P = 0.22$). On average, putative interneurons (denoted by red dots in Fig. 5C) had a shorter latency than wide-spike cells ($P < 0.001$; Kolmogorov–Smirnov test).

To investigate the conditions surrounding the onset and offset of UP states, we averaged the normalized firing rate of all cells in both classes, relative to UP state onset or offset (Fig. 6). Narrow-spike

neurons exhibited robust activity at the onset of so-UP states ($>10 \times$ the mean firing rate), which was phase-locked to the initial LFP oscillation (mean second peak modulation = 1.35; SD = 0.31; see Materials and methods; Fig. 4A and C). For putative pyramidal cells, no modulation was visible in the average PETH, although individual neurons may show modulation at spindle frequency (mean second peak modulation = 0.98; SD = 0.12; cf. Fig. 4G). This finding likely reflects the cancellation of the variable phase modulation preferences for different cells. For tw-UP states, narrow-spike cells exhibited an initial period of approximately 100 ms of sustained activity, but with no rhythmicity (Fig. 6B). The magnitude and dynamics of the activity of wide-spike cells were similar to those during so-UP states (see also Fig. 4F). At the termination of so-UP states, putative interneuron activity fell quickly to zero after the last spindle-like cycle, with putative pyramidal cell firing following immediately after (Fig. 6C). This most likely should not be interpreted as inhibition causing the end of the UP state, but rather that, during the so-UP state, interneurons are more active at the earlier phase of spindle modulation (Fig. 5C). At the termination of tw-UP states, a gradual decay of putative interneuron firing was followed by a delayed decay of putative pyramidal cell firing ($P < 0.001$; paired sign-test of mean firing rates during 60–20 ms before tw-UP state offset; Fig. 6D) which was similar to results reported previously in ferrets (Haider *et al.*, 2006).

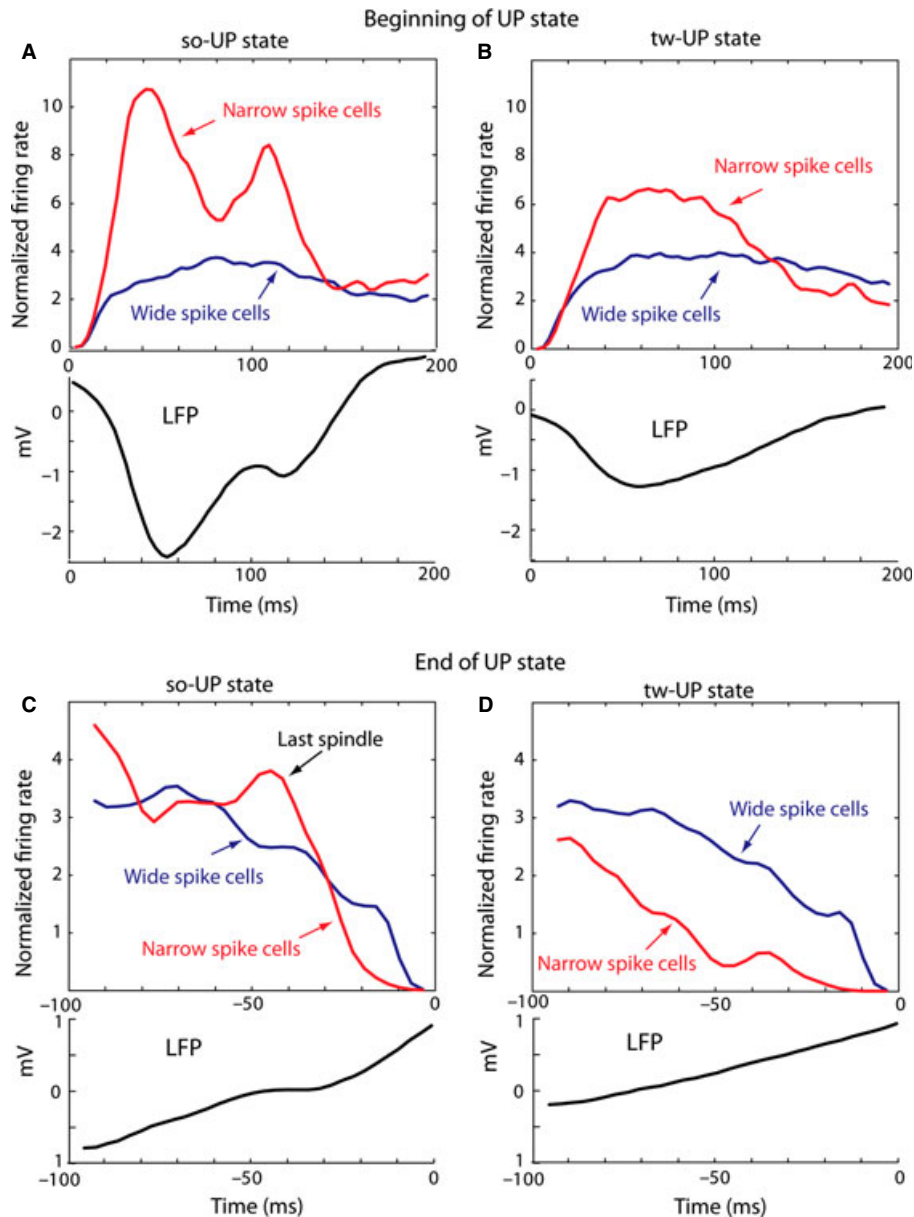


FIG. 6. Normalized firing rate of narrow-spike cells (red) and wide-spike cells (blue) during UP state. (A and B) Normalized activity during the beginning of so-UP states and tw-UP states, respectively. During so-UP states, narrow-spike cells show locking to spindle-frequency modulation; wide-spike cells on average do not show robust modulation at the spindle frequency. (C and D) Normalized activity triggered at the end of so-UP states and tw-UP states, respectively. At the end, activity slowly decreases with narrow-spike cells dying out before wide-spike cells, especially visible in the tw-UP state case.

Discussion

The activity of neuronal populations was analyzed during spontaneous activity in ketamine/xylazine-anesthetized rats. UP states occurred in a variety of forms, ranging from so-UP states accompanied by spindle-frequency modulation to longer-lasting UP states that were usually initiated by traveling waves of activity spreading across the recording shanks (tw-UP states). During so-UP states, narrow-spike cells (putative interneurons) were strongly active and synchronized to the spindle rhythm, whereas wide-spike neurons (putative pyramidal cells) showed no spindle-frequency modulation on average, although individual cells exhibited a diversity of relationships to the extracellular field rhythm. During tw-UP states, narrow-spike cells increased their activity above baseline for approximately 100 ms, after which their rate fell to a constant level for the remainder of the event. Wide-spike

neurons were not as strongly active at UP state onset, but displayed long-lasting sustained activity. UP state termination was characterized by a termination of narrow-spike activity before wide-spike activity. Putative pyramidal cells fired in a reliable order relative to local UP state onset. Remarkably, despite the wide diversity in UP state forms, the sequential order of neuronal recruitment was preserved across UP state types. This suggests that spontaneous activity has a fine, temporally ordered spatial structure where every UP state repeats a similar sequence (pattern) of neuronal activity.

Heterogeneous types of spontaneous activity

Simultaneous-onset events (so-UP states) were accompanied by sharp initial peaks in LFP and spindle-frequency (~ 12 Hz) oscillation. We

propose that these oscillations are homologous to K-complexes. These events occurred almost simultaneously on all recorded channels, and tended to recur rhythmically at approximately 3 Hz (delta frequency). These UP states were usually shorter (~200 ms) than the UP states originally described by Steriade *et al.* (1993a). They were accompanied by strong firing of putative interneurons, phase-locked to the spindle-frequency modulation. Putative pyramidal cells, however, showed a variety of timing profiles. Although some were phase-locked to the initial phase of oscillation, others were active at opposite phases, resulting in a mean profile that was independent of the oscillation. Spiking activity ended abruptly after the last oscillation cycle. The large field potential and strong activation of putative interneurons suggest a sudden, strong synchronizing force arriving simultaneously at a large area of the cortex and may signal thalamic involvement. This hypothesis is further supported by the presence of 12 and 3 Hz oscillations, both known to be generated by thalamic circuits (Steriade *et al.*, 1993b).

At the other extreme, smaller amplitude, longer events were found, the onset of which propagated as a traveling wave in either direction across the recording shanks (tw-UP states). The involvement of cell classes in these events was different, with comparatively less activation of putative interneurons, and a relatively stronger activation of putative pyramidal cells. Putative interneurons fired strongly for the first 100 ms, before relaxing to a lower level steady state. Putative pyramidal cells again showed a diversity of time profiles relative to local event onset. These events died out gradually, with interneuron activity tapering off at approximately 50 ms before pyramidal cell activity. We propose that this type of activity is homologous to the traveling waves observed in isolated cortical slices (Sanchez-Vives & McCormick, 2000), and in human scalp electroencephalography recordings (Massimini *et al.*, 2004), suggesting that this activity may occur through similar mechanisms, i.e. lateral propagation of excitation through pyramidal–pyramidal connections.

Sequential activation of putative pyramidal cells at UP state onsets

All recorded interneurons displayed similar PETH shapes in relation to UP state onset. Putative pyramidal cells, however, showed a wide range of timing behaviors, with some firing rapidly at UP state onset and others beginning to fire after longer latencies. Principal component analysis did not reveal discrete clusters of PETH shapes, but a continuum of behaviors. When viewed as a population, this diversity of onset latencies revealed a progressive spread of activation throughout the neural population. However, this progression was not related to the traveling waves that propagate across recording sites at the onset of tw-UP states, as sequential activation was seen within the pyramidal cells recorded from a single site. Furthermore, latency was not correlated with vertical location on the multi-site electrodes. This finding suggests that it also did not result from horizontally propagating waves relative to an oblique electrode, nor did it reflect a vertical propagation of activity. Sequential activation of putative pyramidal cells was also seen in so-UP states. Also, a comparison of PETH profiles relative to tw-UP state and so-UP state onsets showed that the recruitment sequence of pyramidal cells was similar for both event types. Similar latency sequences have been observed under urethane anesthesia and in awake head-restrained rats (Luczak *et al.*, 2007), in the prefrontal cortex of naturally sleeping rats (Peyrache *et al.*, 2010), and with fast optical recordings in slice preparations (Mao *et al.*, 2001). However, the reliable order of activation latencies that we observe here in average PETHs and cross-correlograms should be distinguished from the

precisely repeating sequences of single spikes that have been claimed in single trials, often at timescales of seconds or more (Abeles *et al.*, 1993; Ikegaya *et al.*, 2004) (but see also Oram *et al.*, 1999).

Significance of different UP state types

We propose that the heterogeneous nature of cortical spontaneous activity reflects distinct mechanisms by which excitation may be propagated in cortical modules. In the first scenario, which we propose underlies tw-UP states, activity propagates laterally through cortico-cortical synapses. Activity emerges at a given cortical site, leading to sustained firing, and subsequently spreads to other sites. Eventually, due to a buildup of synaptic depression, outward currents, and other adaptive factors, the amount of positive feedback at the original site would no longer be sufficient for sustained activity there, and firing would slowly die out. This scheme is similar to that proposed on the basis of slice models of the UP state (Sanchez-Vives & McCormick, 2000).

In the second scenario, which we propose underlies so-UP states, thalamocortical interactions play a critical role in coordinating spontaneous cortical activity. Stronger and more sudden cortical activity can trigger patterns of thalamic oscillations, which may in turn synchronize wide cortical areas. Increased spiking of interneurons would serve to dampen network activity, leading to a shorter duration of recurrent firing. The presence of spindle and delta rhythmicity in these so-UP state events supports thalamic involvement (McCormick & Pape, 1990; Leresche *et al.*, 1991; Steriade *et al.*, 1991; Contreras & Steriade, 1995; Destexhe *et al.*, 1999). We suggest that the larger amplitude cortical events are homologous to the K-complex observed in human scalp electroencephalography. Interestingly, the sequential order of pyramidal cell activation is similar for the two event types, suggesting that by whichever mechanism activity emerges in the neocortex, its spatiotemporal spread within a localized cortical area is similar.

Supporting Information

Additional supporting information can be found in the online version of this article:

Fig. S1. Population recordings and discrimination of putative interneurons and putative pyramidal cells. (A) Schematic of silicone probe with eight recording sites per shank. (B) Average spike waveforms of identified neurons recorded simultaneously at a single shank. Numbers refer to electrode numbering shown in insert in (A). Arrow at the bottom indicates a sample neuron with narrow spikes. Note that using multiple recording sites at one shank allows for multiple neurons to be identified which would be difficult to do with only one recording site. (C) Segregation of putative interneurons (narrow spike cells) and putative pyramidal cells (wide spike cells). Blue and red circles show neurons classified as putative pyramidal cells and putative interneurons, respectively, based on spike duration. For verification of the method, the filled circles denote cells with excitatory (blue) or inhibitory (red) monosynaptic connections. The upper left insert shows normalized average spike waveforms of identified putative interneurons (red) and putative pyramidal cells (blue). Arrows indicate half-amplitude duration and trough to peak time. The trough to peak time was measured up to 1.1 ms. Examples of crosscorrelograms indicating monosynaptic inhibition and excitation are shown in bottom inserts, respectively.

Fig. S2. Interspike interval. Left: Examples of interspike intervals (ISIs) for three putative pyramidal cells (blue) and putative interneurons (red). ISI at the top is characteristic of a bursting cell. Right: Mean ISI (calculated within 100ms) and mean firing rate of recorded

neurons. Note that neurons identified as putative interneurons (red) tend to have higher firing rates and shorter ISIs characteristic for GABAergic fast-spiking cells.

Please note: As a service to our authors and readers, this journal provides supporting information supplied by the authors. Such materials are peer-reviewed and may be re-organized for online delivery, but are not copy-edited or typeset by Wiley-Blackwell. Technical support issues arising from supporting information (other than missing files) should be addressed to the authors.

Acknowledgements

The authors thank Dr K. D. Harris and Dr G. Buzsáki for many helpful comments and for supporting part of this work, and Amanda Mauthe-Kaddoura for proofreading. This work was partly supported by AHFMR and by NSERC (A.L.). The authors declare no conflict of interests.

Abbreviations

LFP, local field potential; PETH, perievent time histogram; so-UP, 'simultaneous-onset' UP; tw-UP, 'traveling-wave' UP.

References

- Abeles, M., Bergman, H., Margalit, E. & Vaadia, E. (1993) Spatiotemporal firing patterns in the frontal cortex of behaving monkeys. *J. Neurophysiol.*, **70**, 1629–1638.
- Amzica, F. & Steriade, M. (1998) Cellular substrates and laminar profile of sleep K-complex. *Neuroscience*, **82**, 671–686.
- Bartho, P., Hirase, H., Monconduit, L., Zugaro, M., Harris, K.D. & Buzsáki, G. (2004) Characterization of neocortical principal cells and interneurons by network interactions and extracellular features. *J. Neurophysiol.*, **92**, 600–608.
- Buzsáki, G. (1989) Two-stage model of memory trace formation: a role for 'noisy' brain states. *Neuroscience*, **31**, 551–570.
- Buzsáki, G. & Draguhn, A. (2004) Neuronal oscillations in cortical networks. *Science*, **304**, 1926–1929.
- Constantinidis, C. & Goldman-Rakic, P.S. (2002) Correlated discharges among putative pyramidal neurons and interneurons in the primate prefrontal cortex. *J. Neurophysiol.*, **88**, 3487–3497.
- Contreras, D. & Steriade, M. (1995) Cellular basis of EEG slow rhythms: a study of dynamic corticothalamic relationships. *J. Neurosci.*, **15**, 604–622.
- Cossart, R., Aronov, D. & Yuste, R. (2003) Attractor dynamics of network UP states in the neocortex. *Nature*, **423**, 283–288.
- Destexhe, A. & Sejnowski, T.J. (2001) *Thalamocortical assemblies how ion channels, single neurons, and large-scale networks organize sleep oscillations*. Oxford University Press, Oxford.
- Destexhe, A., Contreras, D. & Steriade, M. (1999) Cortically-induced coherence of a thalamic-generated oscillation. *Neuroscience*, **92**, 427–443.
- Gomez Palacio Schjetnan, A. & Luczak, A. (2011) Recording large-scale neuronal ensembles with silicon probes in the anesthetized rat. *J. Vis. Exp.*, **56**, e3282.
- Haider, B., Duque, A., Hasenstaub, A.R. & McCormick, D.A. (2006) Neocortical network activity *in vivo* is generated through a dynamic balance of excitation and inhibition. *J. Neurosci.*, **26**, 4535–4545.
- Harris, K.D. (2005) Neural signatures of cell assembly organization. *Nat. Rev. Neurosci.*, **6**, 399–407.
- Harris, K.D., Henze, D.A., Csicsvari, J., Hirase, H. & Buzsáki, G. (2000) Accuracy of tetrode spike separation as determined by simultaneous intracellular and extracellular measurements. *J. Neurophysiol.*, **84**, 401–414.
- Ikegaya, Y., Aaron, G., Cossart, R., Aronov, D., Lampl, I., Ferster, D. & Yuste, R. (2004) Synfire chains and cortical songs: temporal modules of cortical activity. *Science*, **304**, 559–564.
- Kawaguchi, Y. & Kubota, Y. (1997) GABAergic cell subtypes and their synaptic connections in rat frontal cortex. *Cereb. Cortex*, **7**, 476–486.
- Kenet, T., Bibitchkov, D., Tsodyks, M., Grinvald, A. & Arieli, A. (2003) Spontaneously emerging cortical representations of visual attributes. *Nature*, **425**, 954–956.
- Leresche, N., Lightowler, S., Soltesz, I., Jassik-Gerschenfeld, D. & Crunelli, V. (1991) Low-frequency oscillatory activities intrinsic to rat and cat thalamocortical cells. *J. Physiol.*, **441**, 155–174.
- Luczak, A., Barthó, P., Marguet, S.L., Buzsáki, G. & Harris, K.D. (2007) Sequential structure of neocortical spontaneous activity *in vivo*. *PNAS*, **104**, 347–352.
- Luczak, A., Barthó, P. & Harris, K.D. (2009) Spontaneous events outline the realm of possible sensory responses in neocortical populations. *Neuron*, **62**, 413–425.
- MacLean, J.N., Watson, B.O., Aaron, G.B. & Yuste, R. (2005) Internal dynamics determine the cortical response to thalamic stimulation. *Neuron*, **48**, 811–823.
- Mao, B.Q., Hamzei-Sichani, F., Aronov, D., Froemke, R.C. & Yuste, R. (2001) Dynamics of spontaneous activity in neocortical slices. *Neuron*, **32**, 883–898.
- Massimini, M., Huber, R., Ferrarelli, F., Hill, S. & Tononi, G. (2004) The sleep slow oscillation as a traveling wave. *J. Neurosci.*, **24**, 6862–6870.
- McCormick, D.A. & Pape, H.C. (1990) Properties of a hyperpolarization-activated cation current and its role in rhythmic oscillation in thalamic relay neurones. *J. Physiol.*, **431**, 291–318.
- Oram, M.W., Wiener, M.C., Lestienne, R. & Richmond, B.J. (1999) Stochastic nature of precisely timed spike patterns in visual system neuronal responses. *J. Neurophysiol.*, **81**, 3021–3033.
- Peyrache, A., Benchenane, K., Khamassi, M., Wiener, S.I. & Battaglia, F.P. (2010) Sequential reinstatement of neocortical activity during slow oscillations depends on cells' global activity. *Front. Syst. Neurosci.*, **3**, 18.
- Sanchez-Vives, M.V. & McCormick, D.A. (2000) Cellular and network mechanisms of rhythmic recurrent activity in neocortex. *Nat. Neurosci.*, **3**, 1027–1034.
- Schmitzer-Torbert, N., Jackson, J., Henze, D., Harris, K. & Redish, A.D. (2005) Quantitative measures of cluster quality for use in extracellular recordings. *Neuroscience*, **131**, 1–11.
- Sirota, A., Csicsvari, J., Buhl, D. & Buzsáki, G. (2003) Communication between neocortex and hippocampus during sleep in rodents. *Proc. Nat. Acad. Sci. USA*, **100**, 2065–2069.
- Steriade, M. (2001) Impact of network activities on neuronal properties in corticothalamic systems. *J. Neurophysiol.*, **86**, 1–39.
- Steriade, M. & Timofeev, I. (2003) Neuronal plasticity in thalamocortical networks during sleep and waking oscillations. *Neuron*, **37**, 563–576.
- Steriade, M., Dossi, R.C. & Nunez, A. (1991) Network modulation of a slow intrinsic oscillation of cat thalamocortical neurons implicated in sleep delta waves: cortically induced synchronization and brainstem cholinergic suppression. *J. Neurosci.*, **11**, 3200–3217.
- Steriade, M., Contreras, D., Curro Dossi, R. & Nunez, A. (1993a) The slow (< 1 Hz) oscillation in reticular thalamic and thalamocortical neurons: scenario of sleep rhythm generation in interacting thalamic and neocortical networks. *J. Neurosci.*, **13**, 3284–3299.
- Steriade, M., McCormick, D.A. & Sejnowski, T.J. (1993b) Thalamocortical oscillations in the sleeping and aroused brain. *Science*, **262**, 679–685.
- Tsodyks, M., Kenet, T., Grinvald, A. & Arieli, A. (1999) Linking spontaneous activity of single cortical neurons and the underlying functional architecture. *Science*, **286**, 1943–1946.
- Ujjaszasi, J. & Halasz, P. (1986) Late component variants of single auditory evoked responses during NREM sleep stage 2 in man. *Electroencephalogr. Clin. Neurophysiol.*, **64**, 260–268.
- Vertes, R.P. (2004) Memory consolidation in sleep; dream or reality. *Neuron*, **44**, 135–148.
- Viskontas, I.V., Ekstrom, A.D., Wilson, C.L. & Fried, I. (2007) Characterizing interneuron and pyramidal cells in the human medial temporal lobe *in vivo* using extracellular recordings. *Hippocampus*, **17**, 49–57.
- Yokota, T., Eguchi, K. & Hiraba, K. (2010) Functional properties of putative pyramidal neurons and inhibitory interneurons in the rat gustatory cortex. *Cereb. Cortex*, **21**, 597–606.